

# Effect of residual stress and geometric imperfection on the strength of steel box girders

Eun-Ji Jo<sup>1a</sup>, Quang-Viet Vu<sup>2b</sup> and Seung-Eock Kim<sup>\*1</sup>

<sup>1</sup>Department of Civil and Environmental Engineering, Sejong University, 98 Gunja-dong, Gwangjin-gu, Seoul 05006, South Korea

<sup>2</sup>Institute of Research and Development, Duy Tan University, Danang 550000, Vietnam

(Received November 14, 2018, Revised October 17, 2019, Accepted January 4, 2019)

**Abstract.** In the recent years, steel box girder bridges have been extensively used due to high bending stiffness, torsional rigidity, and rapid construction. Therefore, researches related to this girder bridge have been widely conducted. This paper investigates the effect of residual stresses and geometric imperfections on the load-carrying capacity of steel box girder bridges spanning 30 m and 50 m. A three – dimensional finite element model of the steel box girder with a closed section was developed and analyzed using ABAQUS software. Nonlinear inelastic analysis was used to capture the actual response of the girder bridge accurately. Based on the results of analyses, the superimposed mode of webs and flanges was recommended for considering the influence of initial geometric imperfections of the steel box model. In addition, 4% and 16% strength reduction rates on the load – carrying capacity of the perfect structural system were respectively recommended for the girders with compact and non-compact sections, whose designs satisfy the requirements specified in AASHTO LRFD standard. As a consequence, the research results would help designers eliminate the complexity in modeling residual stresses and geometric imperfections when designing the steel box girder bridge.

**Keywords:** residual stress; geometric imperfection; steel box girder; nonlinear inelastic analysis; ABAQUS

## 1. Introduction

Recently, to overcome the problems of ASD and LRFD using linear elastic analysis, a design method using nonlinear inelastic analysis has been proposed in the practical design of AISC (2016), AASHTO-LRFD (2012). However, in these standards, the nonlinear inelastic analysis is only implicitly considered in design equations for a separate member, but not the overall structure system. Due to advances in computer technology, a direct design method using nonlinear inelastic analysis has been employed to analyze the entire structural system. To capture the real behavior of the structure using the nonlinear inelastic analysis, the effect of residual stresses and initial geometric imperfections should be taken into consideration. However, directly modeling residual stresses and geometric imperfections is time-consuming and difficult for the designer.

Several studies have been undertaken to examine the effect of residual stresses and geometric imperfections on the behavior of steel plate and steel box girders (Per Granath 1997, Li *et al.* 2015, Chun and Inoue 2009, Zhang

*et al.* 2016, Graciano *et al.* 2011, Chacón *et al.* 2012, Maiorana and Pellegrino 2018, Saliba *et al.* 2018, Bas 2019). Using the finite element method (FEM), J.A. Chica *et al.* (2013) presented recommendations on imperfections in the design of plated structural elements of bridges subjected to in-plane forces. They found that it was not necessary to use initial residual stresses in the FEM stress patterns based on real measured residual stresses. Additionally, the effect of initial geometric imperfections on the reduction of the ultimate strength obtained from FEM was very important in the case of plated beams subjected to patch loading but no pure shear stress. Graciano *et al.* (2011) conducted an imperfection sensitivity of plate girder webs subjected to patch loading. Based on the analysis results, it was pointed out that initial imperfections for the girder under patch loading can be modeled using either the first eigenmode or sin-wave shape. In most cases in the investigation conducted in Graciano's research, the strength reduction was less than 12% with respect to the idealized web.

Regarding the steel box girder bridges, researches related to this structure have been extensively implemented (Zhou *et al.* 2015, Jiang *et al.* 2013, Liu *et al.* 2016, Hou *et al.* 2015, Maleki *et al.* 2016, Guo *et al.* 2017, Kavehand and Mahjoubi 2017, Kee *et al.* 2018, Vu *et al.* 2018, Kim *et al.* 2018). Vu *et al.* (2018) used the nonlinear inelastic analysis to investigate the impact of intermediate diaphragms on the load-carrying capacity of this girder without considering the influence of residual stresses and geometric imperfections. Kim and Yoo (2008) examined the ultimate strength interaction of rectangular steel box beams using a numerical

---

\*Corresponding author, Professor

E-mail: [sekim@sejong.ac.kr](mailto:sekim@sejong.ac.kr)

<sup>a</sup>MSc.

E-mail: [dytlr1137@gmail.com](mailto:dytlr1137@gmail.com)

<sup>b</sup>Ph.D.

E-mail: [vietvq@vamaru.edu.vn](mailto:vietvq@vamaru.edu.vn)

Table 1 Material properties of steel box components

Component	Type of steel	Yield strength $F_y$ (MPa)	Ultimate strength $F_u$ (MPa)	Modulus of elasticity $E_s$ (MPa)
Webs	SM490	315	490	205,000
Flanges	SM490	315	490	205,000
Longitudinal flange stiffeners	SM490	315	490	205,000
Support diaphragm	SM490	315	490	205,000
Other components	SS400	235	400	205,000

approach, taking into account the effect of residual stresses and geometric imperfections. However, they only investigated these effects for web plate subjected to uniform compression, not the entire girder. Kader (1986) performed a finite element modeling of stiffened steel box girders with imperfections. He suggested that a reduction in strength of about 12% is likely from that of an idealized girder. However, this recommendation can only be used to predict the strength of stiffened steel box girders with an open section that are employed in continuous bridge structures. With the literature review stated above, it is clear that no research related to the effect of residual stresses and geometric imperfections has been implemented for simply supported steel box girder bridges with closed box section.

This paper aims to help designers avoid the complicity in modeling residual stresses and geometric imperfections for design using nonlinear inelastic analysis. Nonlinear inelastic analysis is performed using the commercial software, ABAQUS (2014). 3D finite element models of the steel girder bridges with a closed box section having spans of 30 m and 50 m whose design satisfies the requirement stated in AASHTO LRFD standard (2012), are developed and analyzed. An imperfection sensitivity is conducted to find the appropriate mode shapes for the steel box model, taking the effect of initial geometric imperfections into consideration. The influences of residual stresses, initial geometric imperfections, and the combination of these factors are examined for sixteen girders subjected to symmetrically and eccentrically distributed forces. Finally, strength reduction coefficients on the ultimate strength of the perfect structural system are suggested for the steel box girder bridge.

## 2. Design of steel box girder

Simply supported single span steel box girder bridges are designed corresponding to the AASHTO LRFD standard (2012). The span lengths selected of the girder are 30 m and 50 m for all case study models.

### 2.1 Material properties

In the present study, SM490 steel was used for webs, flanges, longitudinal flange stiffeners, and support diaphragm, while SS400 steel is employed in other components of the steel box girders. The detailed material properties of the steel box components are displayed in Table 1.

### 2.2 Section design

In this section, steel box girder bridges are designed to have non-compact and compact sections, which are commonly used in practical designs.

#### 2.2.1 Span-to-depth ratios

This research only considers the span-to-depth ratios of 20 and 25, as commonly used for simple girders (Hall *et al.* 1999, Coletti *et al.* 2005). Based on these ratios, the girder depths corresponding to span lengths of 30m and 50m were determined.

#### 2.2.2 Webs

Web depths were calculated from the girder depths mentioned above. The minimum web thickness for each case of the girder depth with the non-compact and compact web sections was determined based on the following requirements:

- For webs without longitudinal stiffeners, webs shall be proportioned such that  $D/t_w \leq 150$ , while for webs with longitudinal stiffeners,  $D/t_w \leq 300$  (AASHTO LRFD 2012).
- According to AASHTO/NSBA (2016) steel bridge collaboration, for welded girder construction, the minimum thickness for webs is 12.7 mm to reduce deformation and potential weld defects.
- For the compact web sections, the web thickness must satisfy  $\lambda_{w(D_c)} \leq \lambda_{pw}$ , where  $\lambda_{w(D_c)}$  and  $\lambda_{pw}$  are the slenderness ratio for the web based on the plastic moment and limiting slenderness ratio for a compact web, respectively. For the non-compact web sections, the web thickness must satisfy  $\lambda_{w(D_c)} \leq \lambda_{rw}$ , where  $\lambda_{w(D_c)}$  and  $\lambda_{rw}$  are the slenderness ratio for the web based on the elastic moment and limiting slenderness ratio for a non-compact web, respectively. These above ratios are determined based on the requirement A6.2.1 and A6.2.2 in AASHTO LRFD (2012) as follows

$$\lambda_{w(D_c)} = 2D_{cp} / t_w \quad (1)$$

$$\lambda_{pw} = \frac{\sqrt{E / F_y}}{(0.54M_p / R_h / M_y - 0.09)^2} \quad (2)$$

$$\lambda_{rw} = 5.7\sqrt{E/F_y} \quad (3)$$

Based on Eqs. (1)-(3), the classification of the web shape for all girder types is presented in Tables 2 and 3.

### 2.2.3 Flanges

Regarding top flanges of the box section, the top flange width should satisfy  $b_{ft} \geq \frac{D}{6}$ . The top flange thicknesses of the non-compact and compact flanges were selected to be a minimum value, which satisfies the following requirements mentioned in AASHTO LRFD (2012):

- $t_f \geq 1.1t_w$
- $\frac{b_{ft}}{2t_f} \leq 24$
- The minimum thickness for flanges is 15.875 mm
- For compact flanges, the flange thickness must satisfy  $\lambda_f \leq \lambda_{pf}$ . While for the non-compact flanges, the flange thickness must meet the required  $\lambda_{pf} \leq \lambda_f \leq \lambda_{rf}$ , where,  $\lambda_f$ ,  $\lambda_{rf}$ ,  $\lambda_{pf}$  are the slenderness ratio for the compression flange, limiting the slenderness ratio for non-compact and compact sections, respectively. These above ratios are determined based on requirement A6.3.2 in AASHTO LRFD (2012) as follows

$$\lambda_f = \frac{b_{fc}}{2t_{fc}} \quad (4)$$

$$\lambda_{pf} = 0.38\sqrt{E/F_{yc}} \quad (5)$$

$$\lambda_{rf} = 0.95\sqrt{Ek_c/F_{yr}} \quad (6)$$

Based on Eqs. (4)-(6), the classification of the flange shape for all girder types is presented in Tables 2 and 3.

For the bottom flange, the width was selected as 3000mm - a general limit for the beam web spacing used in the practical design (Musa and Diaz 2007). Besides, the designated bottom flange also had the same thickness as the top flange.

### 2.2.4 Diaphragms

For the span length of 50 m, the spacing of intermediate diaphragms was selected to be 12.2 m, which is the maximum value specified in AASHTO LRFD (2012). Regarding the span length of 30 m, since the intermediate diaphragm is generally placed at the mid-span of the girder bridge in the practical design, three intermediate diaphragms with the spacing of 7.5 m were used. The thickness of the intermediate diaphragms was 8 mm, fulfilling the minimum requirement in AASHTO LRFD (2012). For the support diaphragms, the 24 mm thickness

was applied to prevent fractures due to stress concentration at the boundary conditions.

### 2.2.5 Stiffeners

#### Web Stiffeners

The longitudinal web stiffeners were designed to meet the minimum requirements in AASHTO LRFD (2012), as shown in Eqs. (7) and (8)

$$b_l = 0.48t_s\sqrt{\frac{E}{F_{ys}}} \quad (7)$$

$$I_l = Dt_w \left[ 2.4 \left( \frac{d_0}{D} \right)^2 - 0.13 \right] \beta \quad (8)$$

The stiffeners were located at the optimum position as  $2D_c/5$  from the top flange, as stated in AASHTO LRFD (2012). If the web depth-to-thickness ratio is lower than 150, no longitudinal web stiffener was used.

The transverse web stiffeners were designed in correspondence with certain requirements in AASHTO LRFD (2012) as follows

$$b_l = 2.0 + \frac{D}{30} \quad (9)$$

$$16t_p \geq b_t \geq \frac{b_f}{4} \quad (10)$$

$$I_t \geq I_{t1,2} \quad (11)$$

Based on Eqs. (9)-(11), the detailed web stiffener dimensions for each case study are illustrated.

#### Flange Stiffeners

Longitudinal compression-flange stiffeners on box flanges shall be equally spaced across the flange width. The number of equally spaced longitudinal flange stiffeners,  $n$ , does not exceed five. Based on several practical designs,  $n$  was selected to be 5. The dimensions of longitudinal compression-flange stiffeners were designed to satisfy the following requirements in AASHTO LRFD (2012)

$$b_l = 0.48t_s\sqrt{\frac{E}{F_{yc}}} \quad (12)$$

$$I_l \geq \Psi wt_{fc}^3 \quad (13)$$

Since  $n$  exceeds 2, transverse flange stiffeners are reinforced for flanges. The longitudinal spacing of the transverse flange stiffeners should not exceed three times the full width of the box flange. These stiffeners were designed to meet some requirements in provision C6.11.11.2 in AASHTO LRFD (2012). Based on Eqs. (12) and (13), the details of the flange stiffeners are determined.

Table 2 Classification of the section shape for all girders having 50 m long

Girder type Notation	50L-20D-NcN	50L-20D-NcA	50L-20D-CN	50L-20D-CA	50L-25D-NcN	50L-25D-NcA	50L-25D-CN	50L-25D-CA
Span-depth ratio	20	20	20	20	25	25	25	25
Thickness of web and flange	$t_{minNC}$	$t_{minNC}$	$t_{minC}$	$t_{minC}$	$t_{minNC}$	$t_{minNC}$	$t_{minC}$	$t_{minC}$
Longitudinal web stiffeners	NA*	A*	NA	A	NA	A	NA	A
D	2500	2500	2500	2500	2000	2000	2000	2000
$t_w$	17	16	27	25	14	13	19	19
$\lambda_w$	132	141	83	90	127	136	94	94
$\lambda_{pw}$	91	91	90	90	95	96	94	94
$\lambda_{rw}$	145	145	145	145	145	145	145	145
Section shape	NC	NC	C	C	NC	NC	C	C
$b_f$	455	430	455	430	380	380	380	380
$t_f$	19	18	30	28	16	16	22	22
$\lambda_f$	12	12	8	8	12	12	9	9
$\lambda_{pf}$	10	10	10	10	10	10	9	9
$\lambda_{rf}$	17	17	19	18	17	17	18	18
Section shape	NC	NC	C	C	NC	NC	C	C
Overall section shape	NC*	NC	C*	C	NC	NC	C	C

\*NC: Non-compact section; C: Compact section; NA: None applied; A: Applied

Table 3 Classification of the section shape for all girders having 30 m long

Girder type Notation	30L-20D-NcN	30L-20D-NcA	30L-20D-CN	30L-20D-CA	30L-25D-NcN	30L-25D-NcA	30L-25D-CN	30L-25D-CA
Span-depth ratio	20	20	20	20	25	25	25	25
Thickness of web and flange	$t_{minNC}$	$t_{minNC}$	$t_{minC}$	$t_{minC}$	$t_{minNC}$	$t_{minNC}$	$t_{minC}$	$t_{minC}$
Longitudinal web stiffeners	NA*	A*	NA	A	NA	A	NA	A
D	1500	1500	1500	1500	1200	1200	1200	1200
$t_w$	13	13	13	13	13	13	13	13
$\lambda_w$	97	97	49	49	74	74	37	37
$\lambda_{pw}$	98	98	96	96	99	99	96	96
$\lambda_{rw}$	145	145	145	145	145	145	145	145
Section shape	C	C	C	C	C	C	C	C
$b_f$	380	380	380	380	380	380	380	380
$t_f$	16	16	20	20	16	16	20	20
$\lambda_f$	12	12	6	6	12	12	6	6
$\lambda_{pf}$	10	10	10	10	10	10	10	10
$\lambda_{rf}$	18	18	21	21	19	19	22	22
Section shape	NC	NC	C	C	NC	NC	C	C
Overall section shape	NC*	NC	C**	C	NC	NC	C	C

\*NC: Non-compact section; C: Compact section; NA: None applied; A: Applied

2.2.6 Steel box girder geometries in parametric study

In the current study, sixteen different steel box girders were investigated, as shown in Table 4. The symbols used in the bridge type row in Table 4 represent the concerned designations of the bridge types : L stands for length, D stands for depth, Nc and C stand for the girder with non-compact and compact sections, respectively, and A and N stand for girder webs with and without longitudinal stiffeners, correspondingly. For example, 50L-20D-NcN denotes a steel box girder having a span length of 50 m, span-to-depth of 20, the girder with the non-compact section, and the girder web without longitudinal stiffeners.

Other symbols used in Table 4 are illustrated in Fig. 1 and explained in the notation section.

3. Finite element modeling

In this study, commercial ABAQUS software (2014), version 6.14, was used to analyze the 3D finite element models of the steel box girders, considering nonlinear inelastic analysis. In this section, the material models, element types, contact and boundary conditions, loading conditions, modeling of residual stresses, and geometric imperfections are described.

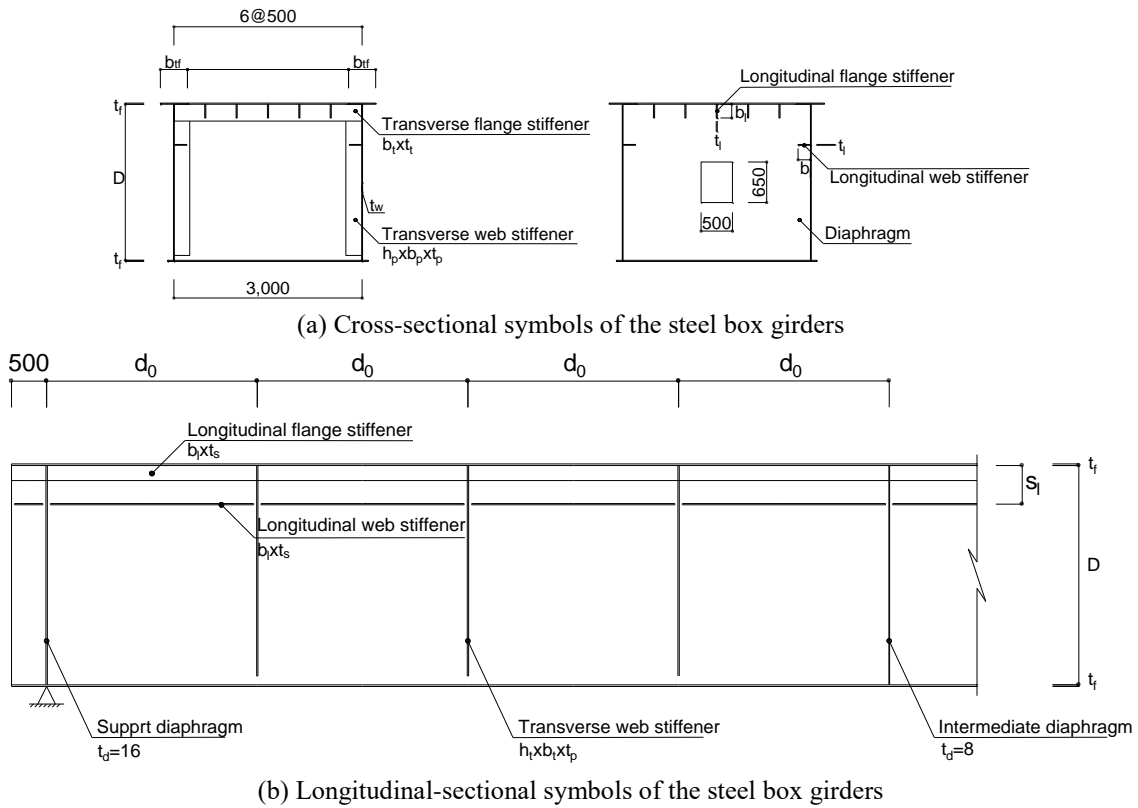


Fig. 1 Symbols of the steel box girders

3.1 Material model

The bilinear stress-strain relationship was used to model the nonlinear behavior of the steel box components, as shown in Fig. 2. To specify the stress-strain curve, the yield strength  $F_{sy}$ , yield strain  $\epsilon_{sy}$ , and the ultimate strength  $F_{su}$  need to be inputted, while the ultimate strain  $\epsilon_{su}$  was assumed to be 0.25.

3.2 Element type and mesh

In the current study, all members of the steel box girders were modeled using S4R elements, which have been commonly used in the modeling of thin-walled structures (Vu *et al.* 2018, 2019a, 2019b, Eom *et al.* 2019, Song *et al.* 2019, Truong *et al.* 2019).

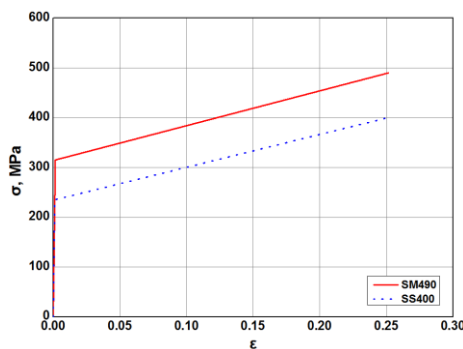


Fig. 2 Stress-strain relationship of the steel models

A sensitivity study of the girder type 50L-20D-CN was conducted to determine appropriate mesh size. The sensitivity analysis results are shown in Table 5 and Fig. 3. It is observed from Fig. 3 when the element size decreases from 3,000 mm to 200 mm, the corresponding ultimate loads converged when the element size of 250 mm was used in the model. There are no further significant changes in ultimate loads when the element size reduces to the value of under 250 mm. In order to save the computation time, the element mesh size of 250 mm was selected for all analyses. The 3D finite element model of the steel box girder is depicted in Fig. 4.

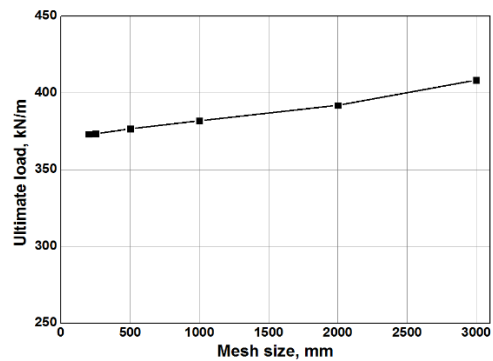


Fig. 3 Sensitivity analysis results



Table 5 Sensitivity analysis result of girder 50L-20D-CN

Mesh size (mm)	3000	2000	1000	500	250	200
Number of Elements	2,076	2,940	3,804	6,734	15,834	21,150
Ultimate load (kN/m)	408.47	392.03	384.94	376.69	373.44	372.93

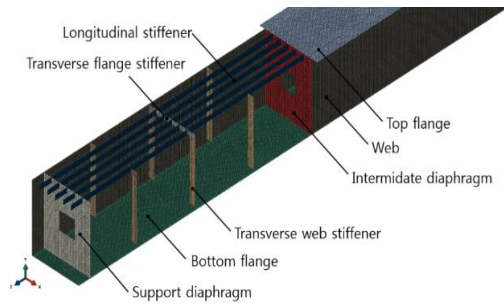


Fig. 4 3D finite element models of the steel box girder in ABAQUS

### 3.3 Contact and boundary conditions

All components of the steel box were assembled to make the complete girder bridge model (Vu *et al.* 2018). There were two different boundary constraints considered in modeling the simply supported box girder bridges including the hinge and roller supports. The support conditions were applied for all nodes at the connection between the support diaphragms and the bottom flange. The roller support was modeled by constraining the movements of the node in the Y direction. The hinge support was restrained from movement in any direction. All supports were allowed to rotate around the support line.

### 3.4 Modeling of residual stresses

The residual stresses considered in the finite element analysis models are shown in Fig.5. This residual stress distribution of the steel box was based on the actual pattern recommended by the European Convention for Constructional Steelwork (ECCS) manual (2012). To take into account the residual stresses, the tensile and compressive stresses in the initial step are directly inputted in the model using the \*PREDEFINED FIELDS option available in ABAQUS (2014). The procedure includes defining several longitudinal partitions of the geometry. Each partition corresponds to a given set of elements that display the same initial stress value. The residual stress patterns are presumed constant along the longitudinal direction of the steel box girder. In this case, the tensile residual stresses of the flange and web at the flange-web juncture were assigned to be  $F_{sy}$ , while the compressive residual stresses of the flange and web were assigned to be  $0.13F_{sy}$ . Generally, flanges and webs of the girder present three partitions (in case only welding is taken into consideration) or alternatively, five partitions (in case both welding and flame-cutting are considered).

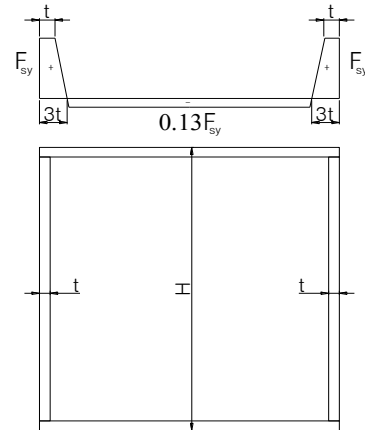


Fig. 5 Residual stress distribution diagram of welded box-section

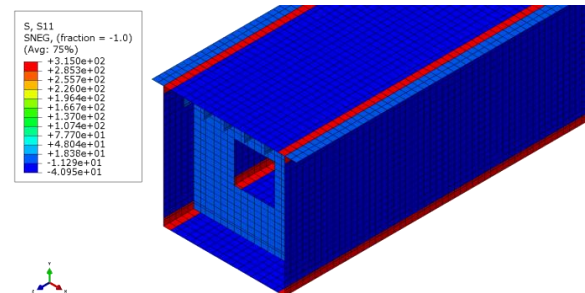


Fig. 6 Residual stresses of the steel box model in Abaqus

Fig. 6 indicates an idealized box girder with a partitioned geometry with only presence of affected stressed zones due to welding in the flange-to-web juncture.

### 3.5 Modeling of geometric imperfections

Geometric imperfection consists of global and local geometric imperfections. In the case of a closed box section, the lateral torsional buckling mode does not occur due to the restraining effect of the box shape and the diaphragm. Therefore, only the local geometric imperfection was considered in this study. In order to model the initial geometric imperfections, the eigenmodes were firstly obtained from the eigenvalue buckling analysis. After that, these eigenmodes were introduced as initial shapes for nonlinear inelastic analysis. The amplitude of these eigenmodes was taken from Eurocode 3 (2011), as shown in Table 6 and Fig. 7.

Table 6 Size of the local geometric imperfection

Initial imperfection types	Element	Shape	Size
Local	Panel or sub-panel	Buckling shape	Minimum (a/200, b/200)

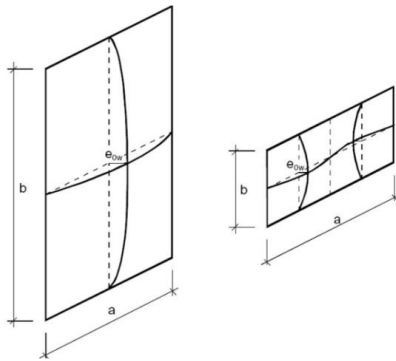
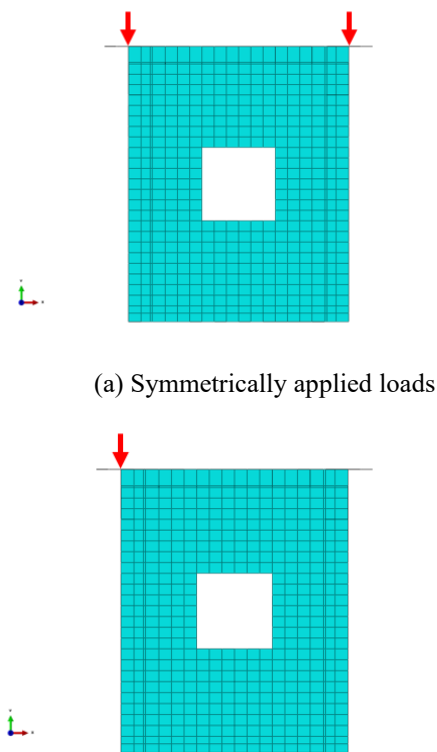


Fig. 7 Local geometric imperfection shapes



(a) Symmetrically applied loads  
(b) Eccentrically applied loads  
Fig. 8 Loading conditions

### 3.6 Loading conditions

In this section, two load cases consisting of symmetrically and eccentrically applied loads were taken into consideration. For the first load case, two lines of uniformly distributed loads were imposed on all nodes of conjunctions between the top flange and the webs, whereas for the second load case, only one line of uniformly distributed loads were applied. The loading conditions are illustrated in Fig. 8.

### 4. Imperfection sensitivity

In this section, a sensitivity analysis was conducted for girders with non-compact (50L-20D-NcA, 30L-20D-NcA) and compact sections (50L-20D-CA, 30L-20D-CA) to investigate the effect of initial geometric imperfections on the load-carrying capacity of the steel box girder. The following analyses were implemented:

- Using the shape of eighth buckling mode (eigenmode) consisting of the first eigenmode (Mode 1), the second eigenmode (Mode 2), the third eigenmode (Mode 3), the summation of the first three eigenmodes (Mode 1 + 2 + 3), the mode shape of webs (Web), the mode shape of top flange (Top flange), the mode shape of bottom flange (Bottom flange), the combination of the mode shapes of webs and flanges (Webs + flanges).
- The imperfection amplitude was selected to be equal to  $hw/200$ , which is the maximum allowable tolerance in the EC3-Part 1.5 (2011).

Figs. 9 and 10 show the influence of varying the initial shape imperfection on the load-displacement behaviors, while Table 7 presents the ultimate strengths according to various imperfection shapes of the girder with non-compact and compact sections in four case studies. Regarding the non-compact sections, it can be observed from these figures that when the Mode 1, 2, 3, 1 + 2 + 3, web, and bottom flange are considered, the ultimate strength decreases insignificantly. However, there is a remarkable reduction in the ultimate strength when the mode shape of the top flange or combination of mode shapes of webs and flanges are taken into account. For instance, regarding the girder 50L-20D-NcA, it is witnessed from Table 7 that there is a 10.2% reduction in the ultimate load of the perfect system when the mode shapes of webs and flanges are considered. For the compact sections, no significant change in the ultimate strength appears. The buckling mode shapes of the girder with non-compact and compact sections are presented in Figs. 11 and 12.

From Table 7, it is worth noting that a superimposed mode has a greater effect on the strength reduction that does modes considered separately. This is also mentioned in the research by Kader (1986) on the steel girder with open box section. It is clear from Table 7 that the summation of mode shapes of webs and flanges give the lowest prediction of the ultimate strength for both non-compact and compact sections. Therefore, a superimposed mode of webs and flanges are recommended for the steel box model considering the effect of initial geometric imperfections.

Table 7 Ultimate strengths according to various imperfection shapes of the non-compact and compact sections

Girder type	Perfect system (kN/m)	Geometric imperfect system (kN/m)							
		Mode1	Mode2	Mode3	Mode 1+2+3	Web	Top flange	Bottom flange	Webs + flanges
50L-20D-NcA	216.74	216.69	216.72	216.73	215.49	215.13	197.08	215.43	196.74
50L-20D-CA	353.89	352.49	353.91	353.07	352.20	352.40	347.69	352.44	347.49
30L-20D-NcA	270.23	270.03	270.17	270.03	270.00	269.99	256.67	270.03	256.31
30L-20D-CA	332.50	332.04	332.65	332.24	331.99	331.90	329.73	330.49	328.70

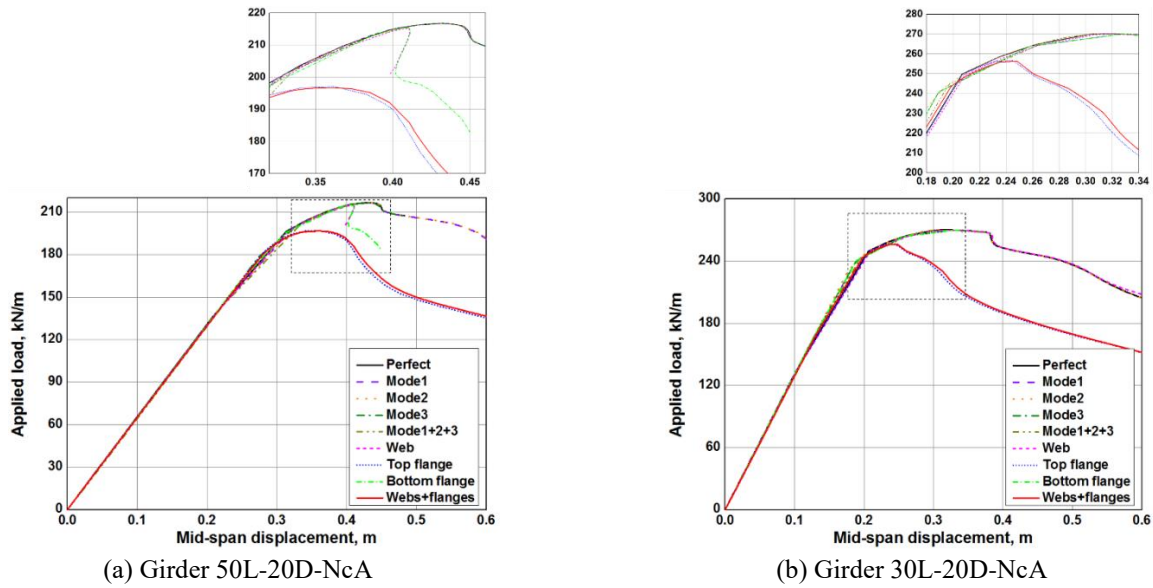


Fig. 9 Load-displacement responses for various imperfection shapes of girders with a non-compact section

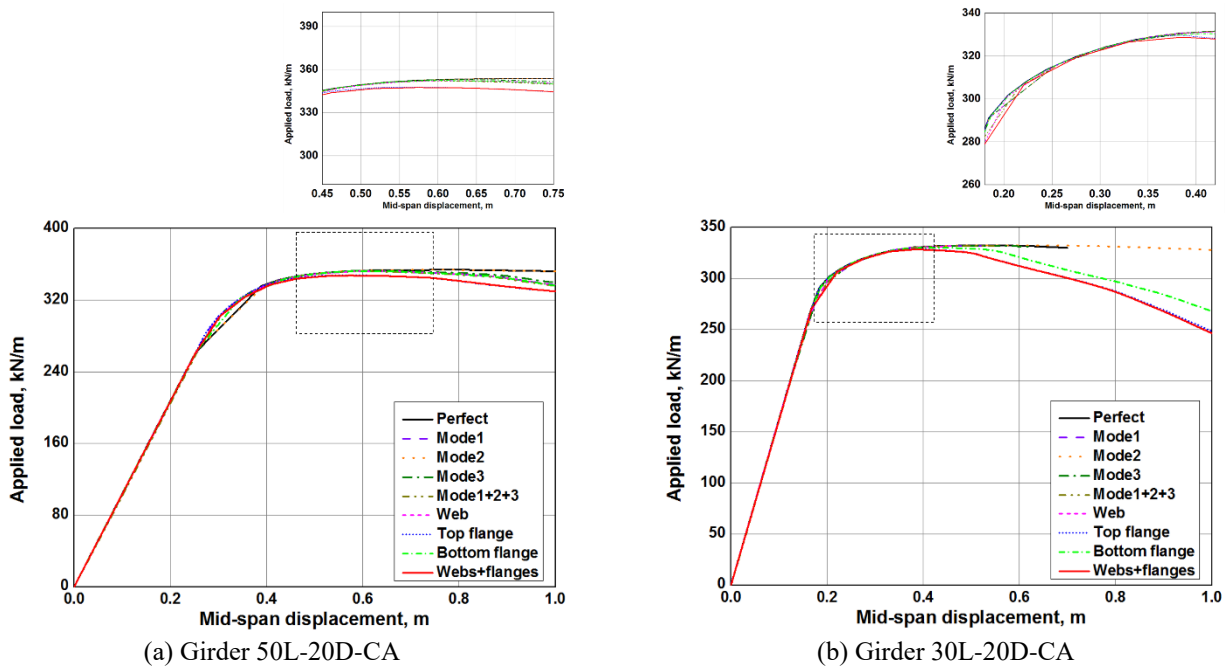


Fig. 10 Load-displacement responses for various imperfection shapes of girders with compact section

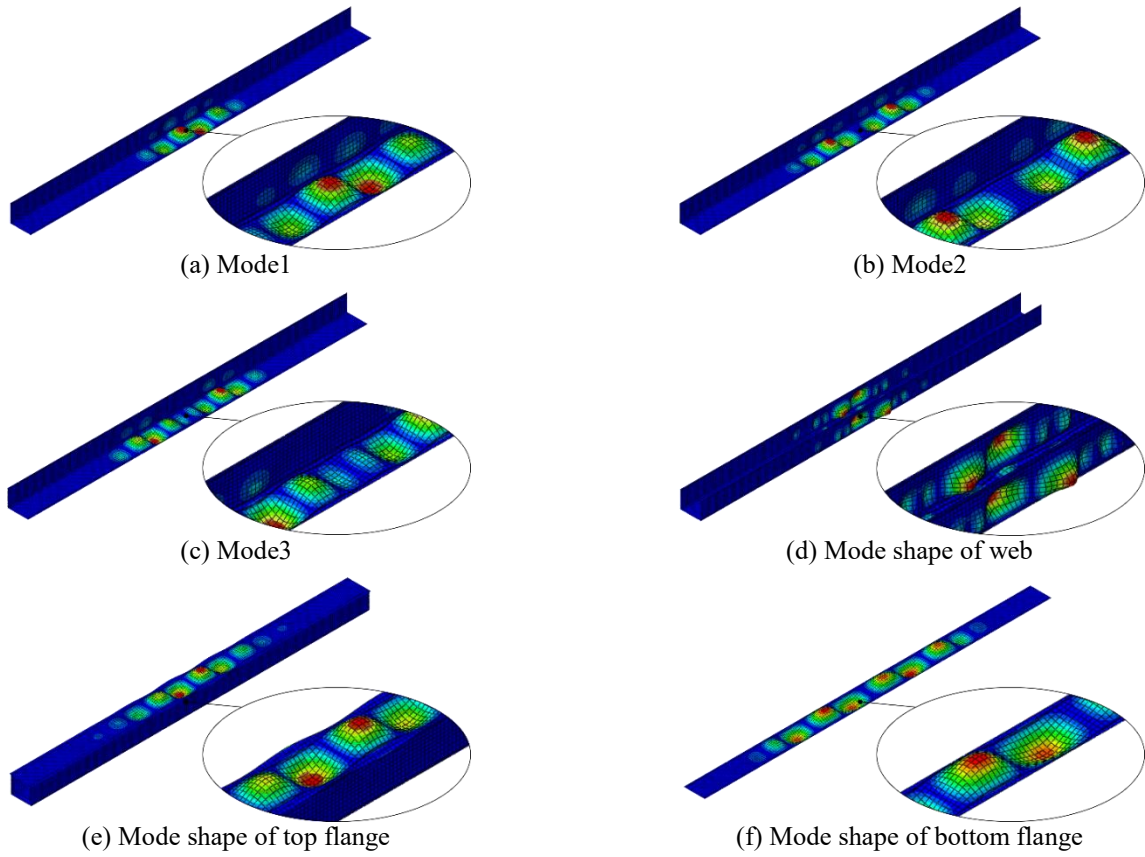


Fig. 11 Buckling mode shapes of the girder with non-compact section (50L-20D-NcA)

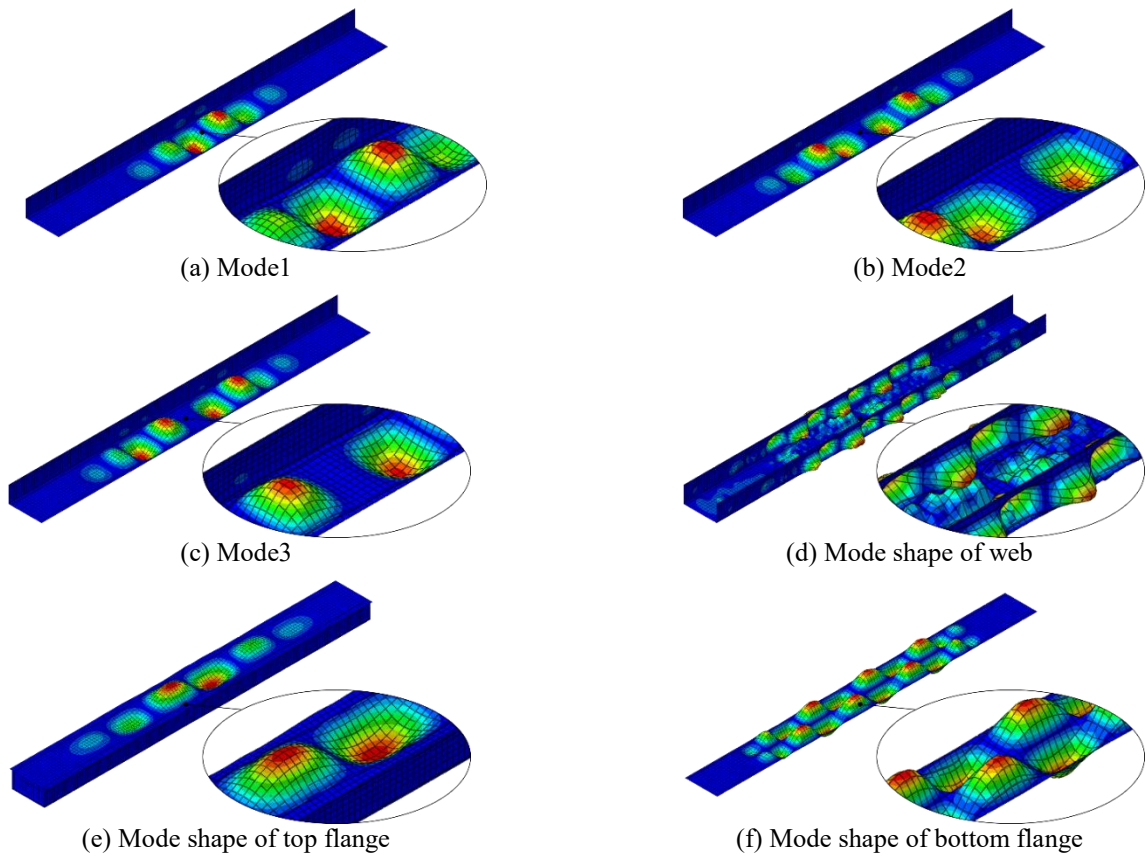
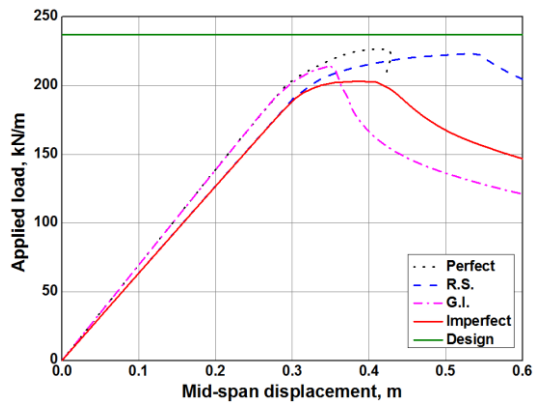
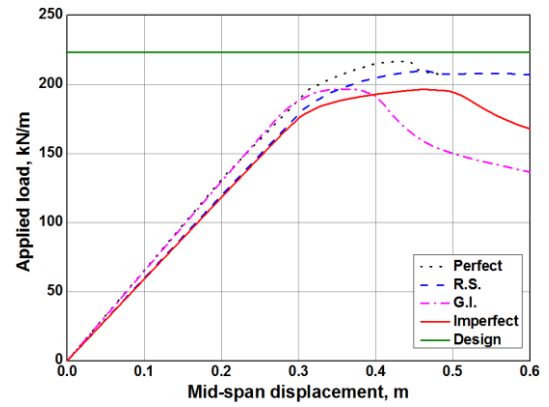


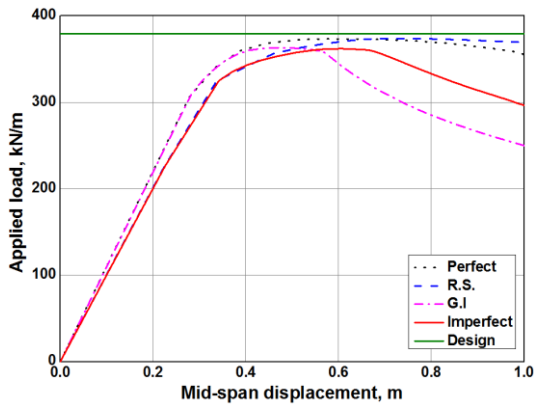
Fig. 12 Buckling mode shapes of the girder with compact section (30L-20D-CA)



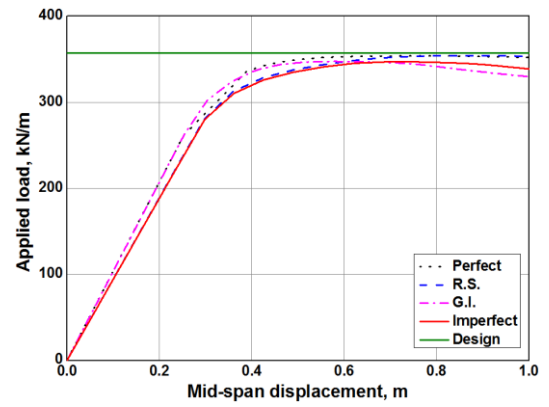
(a) 50L-20D-NcN



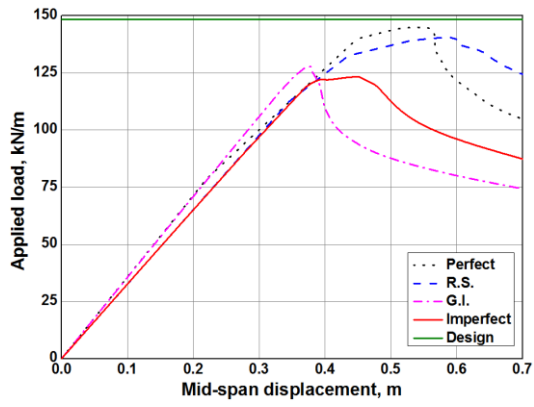
(b) 50L-20D-NcA



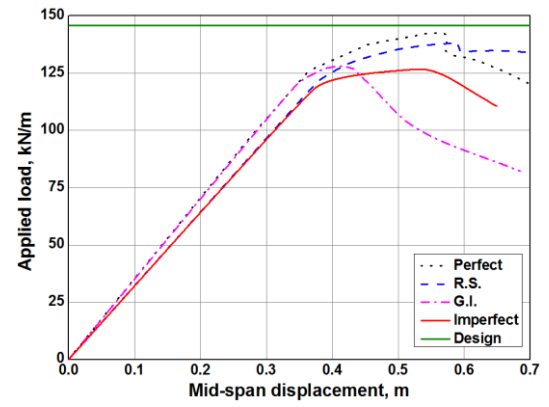
(c) 50L-20D-CN



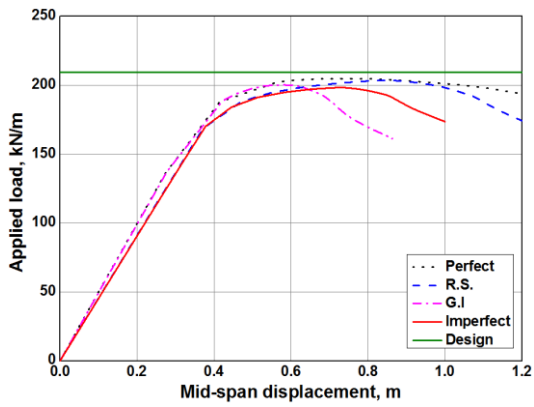
(d) 50L-20D-CA



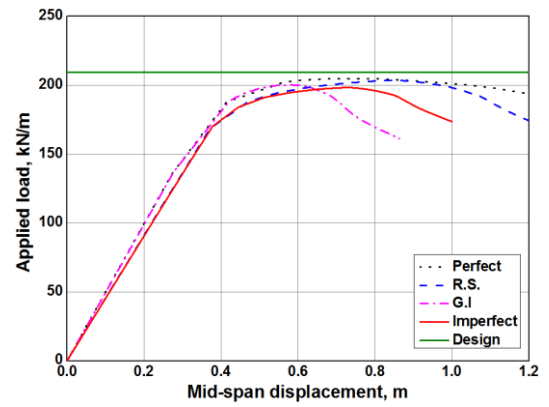
(e) 50L-25D-NcN



(f) 50L-25D-NcA



(g) 50L-25D-CN



(h) 50L-25D-CA

Continued-

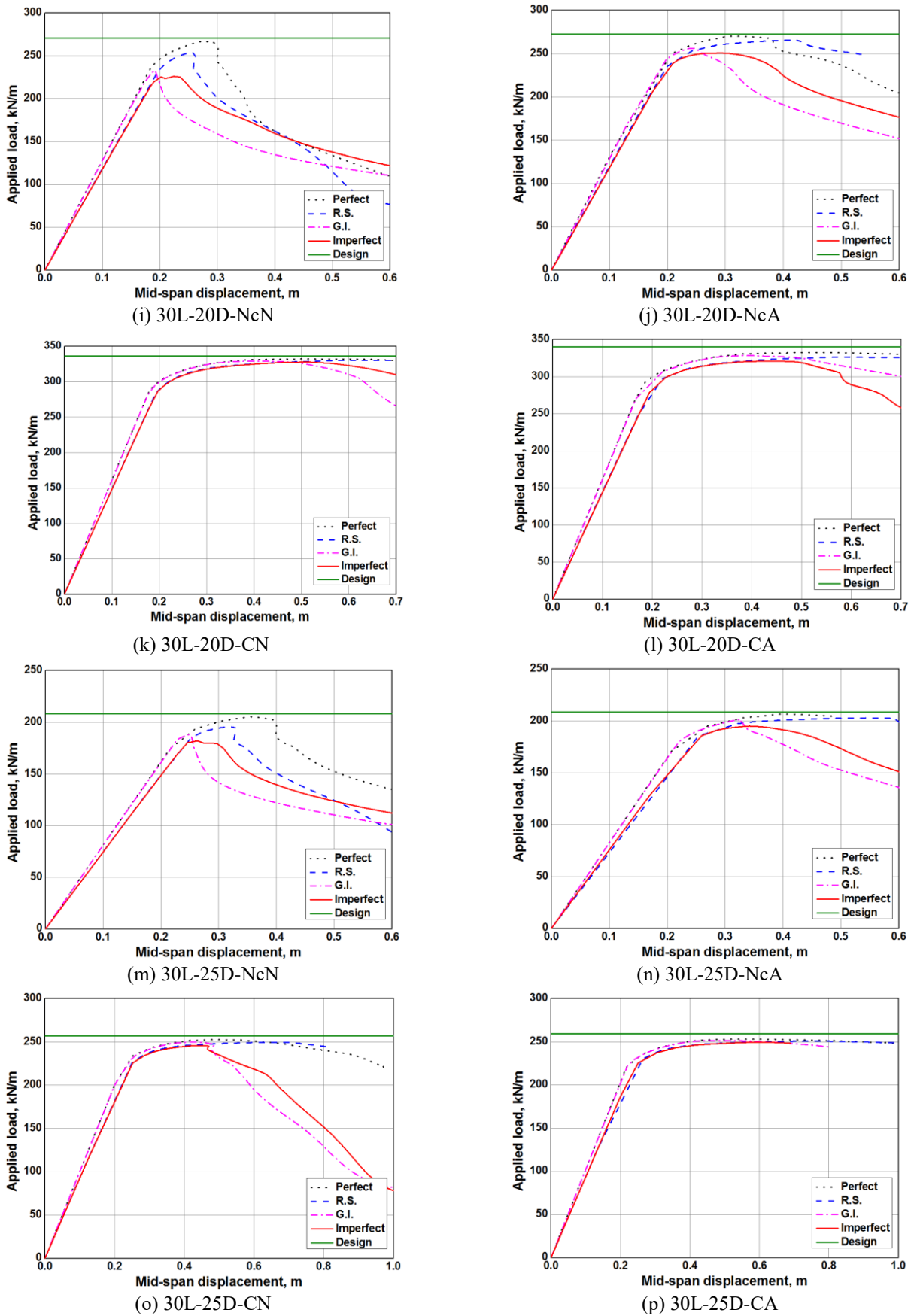


Fig. 13 Comparison of load-displacement curves for various girder types subjected to symmetrically distributed loads

Table 8 Comparison of ultimate strengths of steel box models subjected to symmetrically distributed loads

Girder type	Design	Ultimate strength (kN/m)				Ratio			
		Perfect	R.S.	G.I.	Imperfect	Perfect Design	R. S. Perfect	G. I. Perfect	Imperfect Perfect
50L-20D-NcN	237.26	226.66	223.21	214.12	202.99	0.95	0.98	0.94	0.89
50L-20D-NcA	223.15	216.74	209.83	196.74	196.53	0.97	0.96	0.90	0.90
50L-20D-CN	379.41	373.44	372.99	363.30	362.10	0.98	0.99	0.97	0.96
50L-20D-CA	357.28	353.89	353.16	347.49	347.00	0.99	0.99	0.98	0.98
50L-25D-NcN	148.52	144.92	140.54	127.78	123.37	0.97	0.96	0.88	0.85
50L-25D-NcA	145.84	142.53	137.96	128.01	126.76	0.97	0.96	0.89	0.88
50L-25D-CN	209.52	204.90	203.54	200.36	198.40	0.97	0.99	0.97	0.96
50L-25D-CA	210.29	206.78	206.47	203.57	202.13	0.98	0.99	0.98	0.97
30L-20D-NcN	271.06	267.16	253.64	233.50	226.09	0.98	0.94	0.87	0.84
30L-20D-NcA	272.59	270.23	265.65	256.31	250.80	0.99	0.98	0.94	0.92
30L-20D-CN	336.44	332.29	330.47	329.26	328.06	0.98	0.99	0.99	0.98
30L-20D-CA	340.17	332.50	326.51	328.70	320.95	0.97	0.98	0.98	0.96
30L-25D-NcN	208.45	205.29	195.60	188.24	182.01	0.98	0.95	0.91	0.88
30L-25D-NcA	208.68	206.70	202.98	201.34	195.09	0.99	0.98	0.97	0.94
30L-25D-CN	256.89	252.61	249.64	250.14	245.92	0.98	0.98	0.99	0.97
30L-25D-CA	259.37	253.11	250.93	251.60	249.61	0.97	0.99	0.99	0.98

## 5. Effect of residual stresses and geometric imperfections

In order to investigate the effect of residual stresses and geometric imperfections on the load-carrying capacity of steel box girders, sixteen types of girders subjected to symmetrically and eccentrically distributed loads were examined in these analyses. With each type of the girder, four models are analyzed as described below:

- Model 1: Steel box model without considering the effect of residual stresses and geometric imperfections.
- Model 2: Steel box model considering the effect of residual stresses only.
- Model 3: Steel box model considering the effect of geometric imperfections only.
- Model 4: Steel box model considering the effect of residual stresses and geometric imperfections, simultaneously.

The corresponding results obtained from models 1, 2, 3, and 4 were denoted as Perfect, R.S., G.I., and Imperfect. The design predictions, calculated based on AASHTO LRFD equation (2012), were also used for comparing with these analysis results.

### 5.1 Steel box model subjected to symmetrically distributed loads

Fig. 13 presents a comparison of load-displacement curves, while Table 8 offers a comparison of ultimate strengths of steel box models for sixteen girder types. It can be seen from Table 8 that there is a small difference in the ultimate strengths obtained from the analyses of perfect systems steel box models and the design predictions calculated based on AASHTO LRFD equation (2012). Table 8 shows that the maximum strength reduction rate is 16% obtaining at the girder 30L-20D-NcN when both effects of residual stresses and geometric imperfections are taken into consideration. It is noteworthy from Fig. 13 that for the girders with a non-compact section, the combination of residual stresses and geometric imperfections significantly affects the ultimate strength of the girder, while there is a slight effect on the load-carrying capacity of the girders with a compact section.

In addition, Table 8 shows that geometric imperfections remarkably influence the ultimate strength of the steel box girders with the non-compact section but not for the compact section. When only geometric imperfections are considered, the maximum strength reduction rate is 13% at the girder 30L-20D-NcN, while this ratio is 6% achieving at the same girder when only residual stresses are taken into account. It is found that residual stresses have an insignificant influence on the ultimate strength of the girders with the compact section. It is also noted that the effect of geometric imperfections is higher than that of residual stresses on the load-carrying capacity of the girder in all cases. The failure modes of the steel box models with

and without consideration for the effect of residual stresses and geometric imperfections are shown in Fig. 14.

### 5.2 Steel box model subjected to eccentrically distributed loads

Fig. 15 presents a comparison of load-displacement curves, while Table 9 illustrates a comparison of ultimate strengths of steel box models subjected to eccentrically applied loads. It is found from Table 9 that when the residual stresses are considered, the maximum strength reduction rate is 5% at the girders 50L-25D-NcA and 30L-25D-NcN, but when the geometric imperfections are taken into consideration, this rate is 12% obtaining at the girders 50L-25D-NcN and 30L-20D-NcN. When both influences of residual stresses and geometric imperfections are taken into account, the maximum strength reduction rate achieves the value of 15% at the girder 50L-25D-NcN and 30L-20D-NcN. Additionally, as can be seen in this table, there is a slight effect on the ultimate strength for the girders with the compact section when the residual stresses, geometric imperfections or the combination of them are taken into consideration. The failure modes of the steel box models with and without taking the effect of residual stresses and geometric imperfections into account are displayed in Fig. 16.

### 5.2 Steel box model subjected to eccentrically distributed loads

Fig. 15 presents a comparison of load-displacement curves, while Table 9 illustrates a comparison of ultimate strengths of steel box models subjected to eccentrically applied loads.

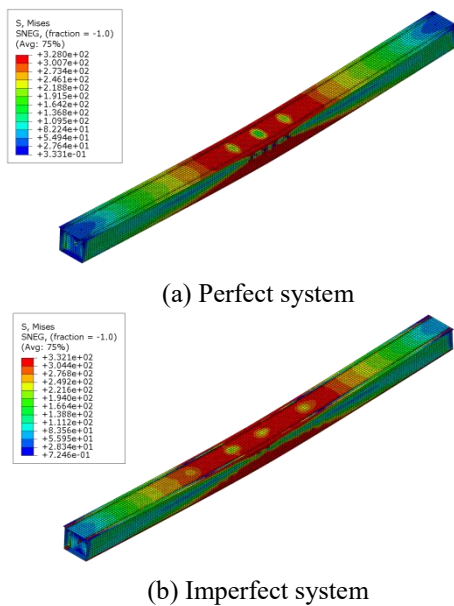


Fig. 14 Failure modes of the girder 50L-20D-CA subjected to symmetrically distributed loads

It is found from Table 9 that when the residual stresses are considered, the maximum strength reduction rate is 5% at the girders 50L-25D-NcA and 30L-25D-NcN, but when the geometric imperfections are taken into consideration, this rate is 12% obtaining at the girders 50L-25D-NcN and 30L-20D-NcN.

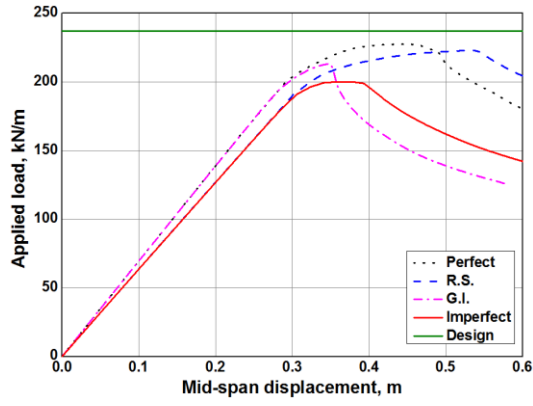
When both influences of residual stresses and geometric imperfections are taken into account, the maximum strength reduction rate achieves the value of 15% at the girder 50L-25D-NcN and 30L-20D-NcN. Additionally, as can be seen in this table, there is a slight effect on the ultimate strength for the girders with the compact section when the residual stresses, geometric imperfections or the combination of them are taken into consideration. The failure modes of the steel box models with and without taking the effect of residual stresses and geometric imperfections into account are displayed in Fig. 16.

Based on the above results, for the steel box models subjected to symmetrically and eccentrically distributed loads, it can be concluded that the maximum strength reduction rates of the girder considering the effects of residual stresses, geometric imperfections, and the combination of them are 6%, 13%, and 16%, respectively. It is noteworthy that the maximum strength reduction rate obtained from this study is 4% higher than that obtained from the research of Kader (1986). The reason for this is that Kader (1986) only considered the steel box with an open section in the negative moment and the steel box dimensions used in his study were not realistic. Moreover, he only investigated the influence of the effects of residual stresses and geometric imperfections for a part of the girder, but not the entire girder, which may lead to some uncertainty in the results. Finally, 4% and 16% strength reduction coefficients for steel box girders with the compact and non-compact sections, respectively, are recommended on the load-carrying capacity of the perfect structural system.

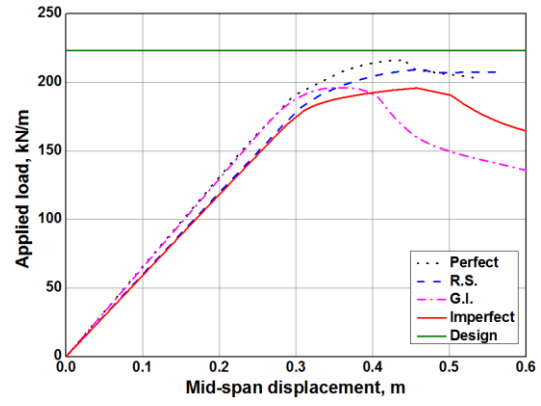
## 6. Conclusions

In the present study, a 3D finite element model of steel box girders spanning of 30m and 50m was developed and analyzed using nonlinear inelastic analysis. The impacts of the residual stresses and geometric imperfections on the load-carrying capacity of the girder bridges are taken into consideration. The results are summarized as follows:

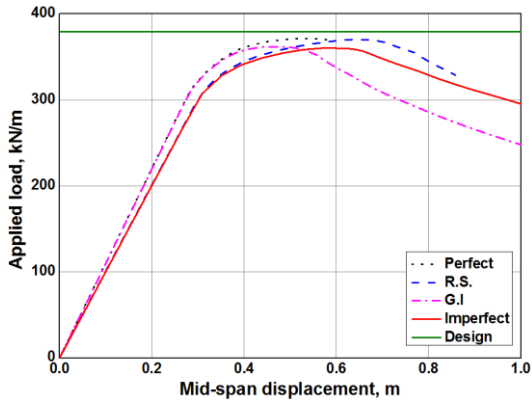
- In modeling an initial imperfection, consideration of a superimposed mode has a greater influence on the strength reduction than separate modes. The superimposed mode of webs and flanges is recommended for the steel box model considering the effect of geometric imperfections.
- The maximum strength reduction rates of the girder with non-compact and compact sections considering the effects of residual stresses, initial geometric imperfections, and a combination of them are 6%, 13%, and 16%, respectively.



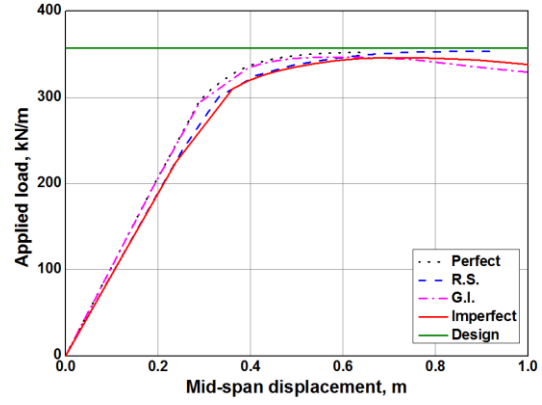
(a) 50L-20D-NcN



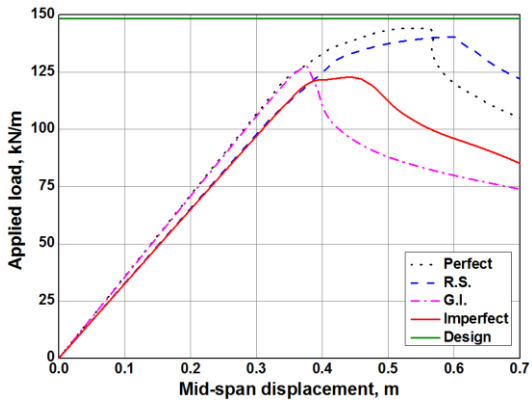
(b) 50L-20D-NcA



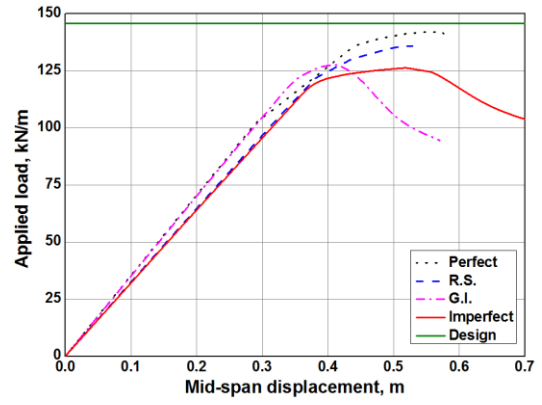
(c) 50L-20D-CN



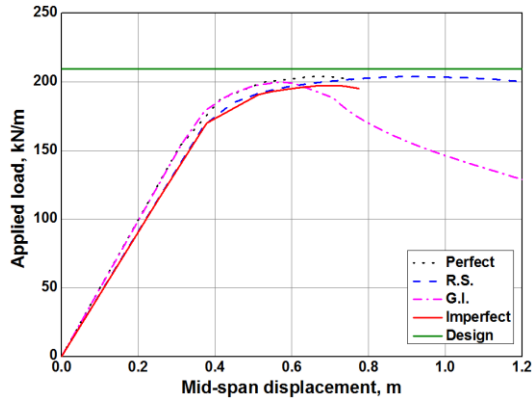
(d) 50L-20D-CA



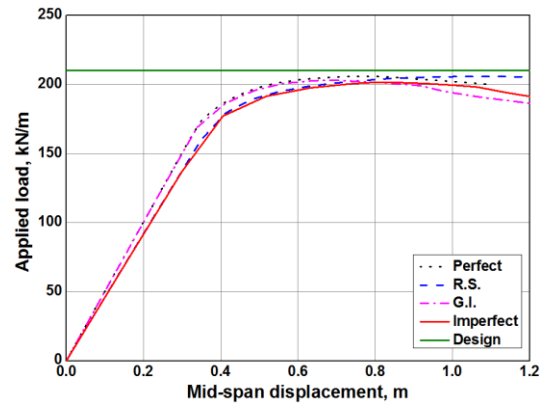
(e) 50L-25D-NcN



(f) 50L-25D-NcA



(g) 50L-25D-CN



(h) 50L-25D-CA

Continued

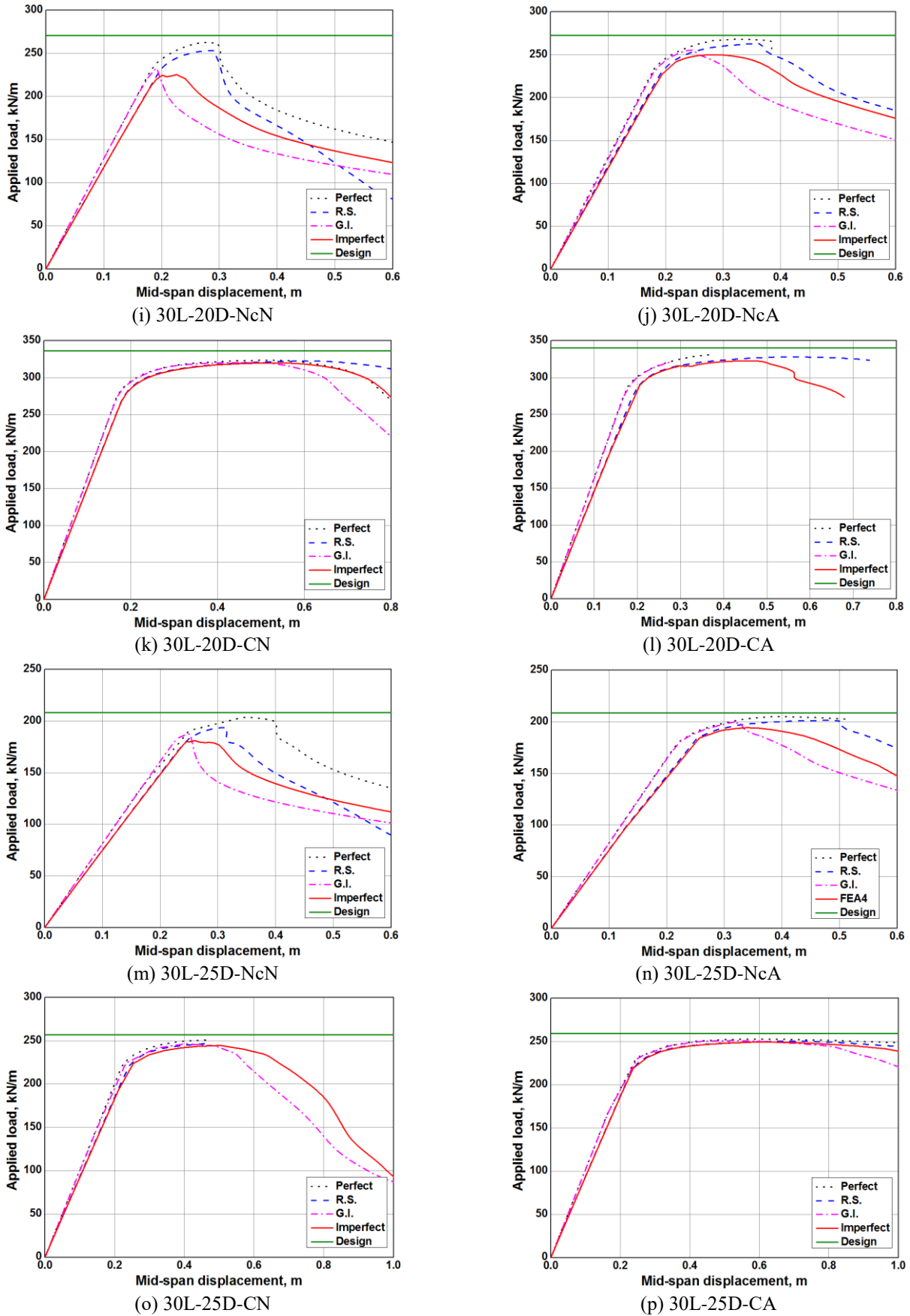


Fig. 15 Comparison of load-displacement curves for various girder types subjected to eccentrically distributed loads

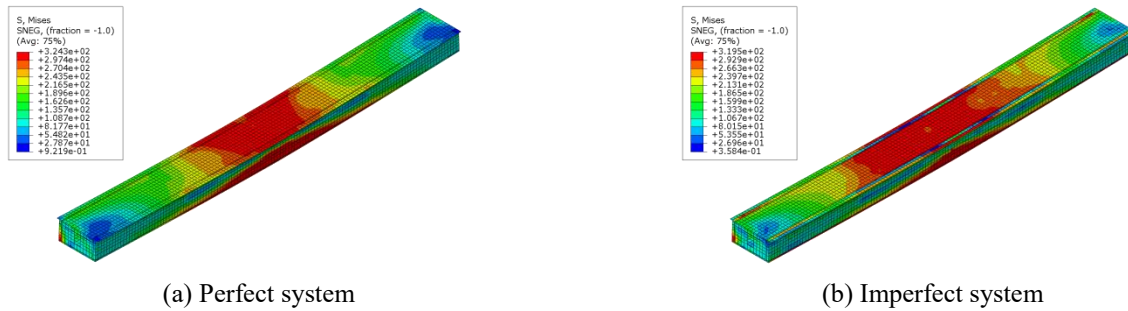


Fig. 16 Failure modes of the 30L-20D-CA girder subjected to eccentrically distributed loads

Table 9 Comparison of ultimate strengths of steel box models subjected to eccentrically distributed loads

Girder type	Design	Ultimate strength (kN/m)				Ratio			
		Perfect	R.S.	G.I.	Imperfect	Perfect Design	R. S. Perfect	G. I. Perfect	Imperfect Perfect
50L-20D-NcN	237.26	224.75	219.00	213.22	200.10	0.94	0.97	0.94	0.89
50L-20D-NcA	223.15	216.21	209.41	196.26	195.96	0.96	0.96	0.90	0.90
50L-20D-CN	379.41	371.41	370.28	361.98	360.33	0.97	0.99	0.97	0.97
50L-20D-CA	357.28	352.12	352.03	346.75	346.10	0.98	0.99	0.98	0.98
50L-25D-NcN	148.52	144.26	140.44	127.42	122.96	0.97	0.97	0.88	0.85
50L-25D-NcA	145.84	142.06	136.04	127.66	126.35	0.97	0.95	0.89	0.88
50L-25D-CN	209.52	204.02	203.81	199.88	197.30	0.97	0.99	0.97	0.96
50L-25D-CA	210.29	205.98	205.86	203.12	201.59	0.97	0.99	0.98	0.97
30L-20D-NcN	271.06	262.88	253.39	233.02	225.39	0.96	0.96	0.88	0.85
30L-20D-NcA	272.59	268.25	263.15	255.47	250.03	0.98	0.98	0.95	0.93
30L-20D-CN	336.44	323.58	322.61	320.66	320.05	0.96	0.99	0.99	0.98
30L-20D-CA	340.17	331.21	328.08	320.74	322.79	0.97	0.99	0.96	0.97
30L-25D-NcN	208.45	203.60	194.05	187.54	181.10	0.97	0.95	0.92	0.88
30L-25D-NcA	208.68	205.03	201.41	200.17	194.42	0.98	0.98	0.97	0.94
30L-25D-CN	256.89	250.72	246.72	246.62	244.76	0.97	0.98	0.98	0.97
30L-25D-CA	259.37	252.88	250.56	251.21	249.59	0.97	0.99	0.99	0.98

- 4% and 16% strength reduction factors on the ultimate strength of the perfect structural system are suggested for steel box girders with the compact and non-compact sections, respectively.
- Based on this study, the complexity of the modeling of the residual stresses and geometric imperfections can be eliminated in designing steel box girder bridges using nonlinear inelastic analysis.

## Acknowledgments

This work was supported by the National Research Foundation of Korea (NRF) grant funded by the Korea

government (MSIT) (No. 2018R1A2A2A05018524) and (No. 2019R1A4A1021702).

## References

- AASHTO LRFD (2012), *AASHTO LRFD Bridge design specifications C.U.S. Units*, American Association of State Highway Transportation Officials; Washington DC, USA.
- AASHTO / NSBA (2016), *Guidelines to Design for Constructability*, American Association of State Highway Transportation Officials / National Steel Bridge Alliance, AASHTO Executive Committee; USA.
- ABAQUS 6.14 (2014), *ABAQUS 6.14 Analysis User's Guide*, ABAQUS 6.14; Dassault Systemes.
- ANSI / AISC 360-16 (2016), *Specification for Structural Steel Buildings*, An American National Standard / American Institute

- of Steel Construction, Illinois; Chicago, USA.
- Bas, S. (2019), "Lateral torsional buckling of steel I-beams: Effect of initial geometric imperfection", *Steel Compos. Struct.*, **30**(5), 483-492. <https://doi.org/10.12989/scs.2019.30.5.483>.
- Chacón, R., Serrat, M., Real, E. (2012), "The influence of structural imperfections on the resistance of plate girders to patch loading", *Thin-Walled Struct.*, **53**, 15-25. <https://doi.org/10.1016/j.tws.2011.12.003>.
- Chica, J.A., José, J.T.S., Millanes, F. and Manso, J.M. (2013), "Recommendations on imperfections in the design of plated structural elements of bridges", *Constr. Steel Res.*, **86**, 183-194. <https://doi.org/10.1016/j.jcsr.2013.04.001>
- Chun, P.J. and Inoue, J. (2009), "Numerical studies of the effect of residual imperfection on the mechanical behavior of heat-corrected steel plates, and analysis of a further repair method", *Steel Compos. Struct.*, **9**(3), 209-221. <https://doi.org/10.12989/scs.2009.9.3.209>.
- Coletti, D., Fan, Z.T., Holt, J. and Vogel, J. (2005), "Practical Steel Tub Girder Design", TRB 2006 Annual Meeting.
- ECCS (2012), European Convention for Constructional Steelwork, European Committee for Standardization; Belgium.
- Eom, S.S., Vu, Q.V., Choi, J.H., Papazafeiropoulos, G., Kim, S.E. (2019), "Behavior of composite CFST beam-steel column joints", *Steel Compos. Struct.*, **32**(5), 583-594. <https://doi.org/10.12989/scs.2019.32.5.583>.
- Eurocode 3 (2011), Design of steel structures. Part 1.5: Plated structural elements, European Committee for Standardization; Brussels, Belgium.
- Graciano, C., Casanova, E. and Martínez, J. (2011), "Imperfection sensitivity of plate girder webs subjected to patch loading", *Constr. Steel Res.*, **67**, 1128-1133. <https://doi.org/10.1016/j.jcsr.2011.02.006>.
- Guo, J., Zheng, S., Zhu, J., Tang, Y., Hong, C. (2017), "Study on post-flutter state of streamlined steel box girder based on 2 DOF coupling flutter theory", *Wind and Structures*, **25**(4), 343-360. <https://doi.org/10.12989/was.2017.25.4.343>.
- Hall, D.H., Grubb, M.A. and Yoo, C.H. (1999), "Improved Design Specifications for Horizontally Curved Steel Girder Highway Bridges", 424; Auburn University.
- Hou, Z., Xia, H., Y. Wang, Zhang, Y. and Zhang, T. (2015), "Dynamic analysis and model test on steel-concrete composite beams under moving loads", *Steel Compos. Struct.*, **18**(3), 565-582. <https://doi.org/10.12989/scs.2015.18.3.565>.
- Jiang, L., Qi, J., Scanlon, A. and Sun, L. (2013), "Distortional and local buckling of steel-concrete composite box-beam", *Steel Compos. Struct.*, **14**(3), 243-265. <https://doi.org/10.12989/scs.2013.14.3.243>.
- Kader, A.A., Korol, R.M. and Mirza, F.A. (1986), "Finite element modeling of stiffened steel box girders with imperfections", Ph.D. Dissertation, McMaster University, Hamilton.
- Kavehand, A. and Mahjoubi, S. (2017), "Design of multi-span steel box girder using lion pride optimization algorithm", *Smart Struct. Syst.*, **20**(5), 607-618. <https://doi.org/10.12989/sss.2017.20.5.607>.
- Kim, K. and Yoo, C.H. (2008), "Ultimate strengths of steel rectangular box beams subjected to combined action of bending and torsion", *Eng. Struct.*, **30**, 1677-1687. <https://doi.org/10.1016/j.engstruct.2007.11.011>
- Kim, J., Kee, S.H., Youn, H. and Kim, D.Y. (2018), "Parameters influencing redundancy of twin steel box-girder bridges", *Steel Compos. Struct.*, **29**(4), 437-456. <https://doi.org/10.12989/scs.2018.29.4.437>.
- Li, T.J., Liu, S.W. and Chan, S.L. (2015), "Cross-sectional analysis of arbitrary sections allowing for residual stresses", *Steel Compos. Struct.*, **18**(4), 985-1000. <https://doi.org/10.12989/scs.2015.18.4.985>.
- Liu, J., Ding, F.X., Liu, X.M. and Yu, Z.W. (2016), "Study on flexural capacity of simply supported steel-concrete composite beam", *Steel Compos. Struct.*, **21**(4), 829-847. <https://doi.org/10.12989/scs.2016.21.4.829>.
- Maiorana, E. and Pellegrino, C. (2018), "Linear elastic behavior of circular holed steel box sections under compression", *Int. J. Steel Struct.*, **18** (3), 1063-1082. <https://doi.org/10.1007/s13296-018-0042-x>.
- Maleki, S., Mohammadinia, P. and Dolati, A. (2016), "Numerical study of steel box girder bridge diaphragms", *Earthq. Struct.* **11**(4), 681-699. <https://doi.org/10.12989/eas.2016.11.4.681>.
- Musa, Y.I. and Diaz, M.A. (2007), "Design Optimization of Composite Steel Box Girder in Flexure", *Pract. Period. Struct. Des. Constr.*, **12**(3), 146-152. [https://doi.org/10.1061/\(ASCE\)1084-0680\(2007\)12:3\(146\)](https://doi.org/10.1061/(ASCE)1084-0680(2007)12:3(146)).
- Per Granath (1997), "Behavior of slender plate girders subjected to patch loading", *Constr. Steel Res.*, **42** (1), 1-19. [https://doi.org/10.1016/S0143-974X\(97\)00021-7](https://doi.org/10.1016/S0143-974X(97)00021-7)
- Saliba, N.G., Tawk, I. and Gergess, A.N. (2018), "Finite element modeling of rolled steel shapes subjected to weak axis bending", *Steel Compos. Struct.*, **29**(2), 161-173. <https://doi.org/10.12989/scs.2018.29.2.161>.
- Song, Y., Uy, B. and Wang, J. (2019), "Numerical analysis of stainless steel-concrete composite beam-to-column joints with bolted flush endplates", *Steel Compos. Struct.*, **33**(1), 975-994. <https://doi.org/10.12989/scs.2019.33.1.143>.
- Truong, V.H., Papazafeiropoulos, G., Pham, V.T. and Vu, Q.V. (2019), "Effect of multiple longitudinal stiffeners on ultimate strength of steel plate girders", *Structures*, **22**, 366-382. <https://doi.org/10.1016/j.istruc.2019.09.002>.
- Vu, Q.V., Thai, D.K. and Kim S.E. (2018), "Effect of intermediate diaphragms on the load - carrying capacity of steel - concrete composite box girder bridges", *Thin-Wall. Struct.*, **122**, 230-241. <https://doi.org/10.1016/j.tws.2017.10.024>.
- Vu, Q.V., Papazafeiropoulos, G., Graciano, C. and Kim S.E. (2019), "Optimum linear buckling analysis of longitudinally multi-stiffened steel plates subjected to combined bending and shear", *Thin-Wall. Struct.*, **136**, 235-245. <https://doi.org/10.1016/j.tws.2018.12.008>.
- Vu, Q.V., Truong, V.H., Papazafeiropoulos, G., Graciano, C. and Kim S.E. (2019), "Bend-buckling strength of steel plates with multiple longitudinal stiffeners", *Constr. Steel Res.*, **158**, 41-52. <https://doi.org/10.1016/j.jcsr.2019.03.006>
- Zhang, X., Liu, S., Zhao, M. and Chiew, S.P. (2016), "Residual stress of cold-formed thick-walled steel rectangular hollow sections", *Steel Compos. Struct.* **22**(4), 837-853. <https://doi.org/10.12989/scs.2016.22.4.837>.
- Zhou, W., Li, S., Jiang, L. and Huang, Z. (2015), "Distortional buckling calculation method of steel-concrete composite box beam in negative moment area", *Steel Compos. Struct.*, **19**(5), 1203-1219. <https://doi.org/10.12989/scs.2015.19.5.1203>.